ELSEVIER Nuclear Instruments and Methods in Physics Research B 147 (1999) 399–409

NIM B Beam Interactions with Materials & Atoms

Glancing incidence diffuse X-ray scattering studies of implantation damage in Si

K. Nordlund [a,*], P. Partyka [b], Y. Zhong [b], I.K. Robinson [b], R.S. Averback [b], P. Ehrhart [c]

[a] Accelerator Laboratory, P.O. Box 43, University of Helsinki, FIN-00014, Helsinki, Finland
[b] Materials Research Laboratory, University of Illinois, Urbana, IL 61801, USA
[c] Institut für Festkörperforschung, Forschungszentrum Jülich, D-5170 Jülich, Germany

Abstract

Diffuse X-ray scattering (DXS) at glancing incidence is a potentially powerful means for elucidating damage structures in irradiated solids. Fundamental to the analysis of diffuse X-ray scattering data is a knowledge of the atomic displacement field around defects, which for implantation damage in crystals like Si has been difficult to obtain using analytical solutions of elastic continuum theory. We present a method for predicting the diffuse scattering pattern by calculating the displacement field around a defect using fully atomistic simulations and performing discrete sums for the scattering intensity. We apply the method to analyze experimental DXS results of defects produced by 4.5 keV He and 20 keV Ga irradiations of Si at temperatures of 100–300 K. The results show that the self-interstitial in ion-irradiated Si becomes mobile around 150 K, and that amorphization of silicon by light and medium-heavy projectiles occurs homogeneously through the buildup of interstitial clusters, and not within single cascade events. © 1999 Elsevier Science B.V. All rights reserved.

PACS: 61.72.Dd; 66.30.Fq; 61.82.Fk; 61.72.Ji
Keywords: Silicon; Defect; Defect clusters; Amorphization; Diffuse X-ray scattering

1. Introduction

Intrinsic defects in silicon have a central role in many aspects of ion implantation processing of semiconductors, notably the annealing and transient-enhanced diffusion behavior [1]. Despite the immense technological interest in these defects, many of their properties have remained elusive. For instance, the structure of the self-interstitial has still not been determined experimentally, although ab initio computer simulations now strongly indicate it has the 1 1 0 dumbbell structure [2]. Even the structure of the vacancy is not fully clear: recent density-functional theory simulations suggest the vacancy has a split structure in the doubly-negative charge state [3]. The migration properties of the vacancy and interstitial have long been unclear, with enormous spreads in diffusivity

* Corresponding author. Tel.: +358 9 19140007; fax: +358 9 19140042; e-mail: kai.nordlund@helsinki.fi

0168-583X/98/$ – see front matter © 1999 Elsevier Science B.V. All rights reserved.
PII: S0168-583X(98)00546-1

values determined by different groups and methods [4]. Although some consensus has begun to emerge for the high-temperature self-diffusion recently [5], it is clear that obtaining new experimental data is desirable for clarifying the situation. The same is true for settling the long controversial question of whether silicon amorphizes by homogeneously (through buildup of defect clusters and a subsequent phase-transformation-like collapse) or heterogeneously (through the growth of amorphous zones).

The migration properties of intrinsic point defects have been studied by a variety of techniques. The results of electron paramagnetic resonance (EPR) and deep-level transient spectroscopy (DLTS) have been recently summarized by Watkins [6]. Positron techniques have also proved to be useful in studying the properties of vacancy-like defect complexes [7]. Common to these methods is that the results are dependent on the electronic structure of the defects. While this can be highly beneficial for instance in determining the electric activation of impurities, it also can make the deduction of the atomic structure of defects complicated. Particularly treating the silicon self-interstitial has proved to be complicated since it is not directly visible by most methods [6]. Diffuse X-ray scattering (DXS) studies of defects, on the other hand, depend only on the atomic arrangement of a defect and the atoms surrounding it. Recent DXS results on defects produced by electron irradiation differ in some respects strongly from the results of "electronic" methods, most notably in that they predict much larger defect introduction rates than previous studies [8].

Although the DXS method is well established [9], it has not been used very much in ion irradiated semiconductors. In the present work, we use a new atomistic analysis method of diffuse X-ray scattering distributions to study intrinsic defects in silicon. Since the analysis method is new, we first present the principles underlying it and simulation results defect clusters. As an example of how the simulations can be useful, these results are then used for interpreting experimental results of He and Ga implanted Si [10,11].

2. Diffuse X-ray scattering analysis

2.1. Background

The "diffuse" part of an X-ray scattering distribution is the (usually very weak) part of the scattering between Bragg peaks. Since defects in a crystal produce strain fields in the lattice surrounding them, they cause a diffuse part to the X-ray scattering. The fundamentals of this scattering process are well understood from analytical scattering theory [9], and a good brief introduction to how DXS arises from defects has been given in Ref. [8]. Here we only point out that the DXS method is attractive for defect studies in that it allows the determination of the exact atomic structure of defects, cluster sizes and relaxation volumes.

The DXS method has been widely used in metals over a long period of time (see e.g. [12] and references therein). DXS measurements of semiconductors are mostly more recent [8,13–16], and have to some extent been hampered by difficulties in interpreting the experimental results. This is partly due to the almost perfect cancellation of vacancy and interstitial relaxation volumes in most semiconductors [13,14]. Hence lattice parameter changes, which are easily observed in metals, cannot be used in semiconductors for distinguishing the interstitial and vacancy. Furthermore, since defects in semiconductors tend to be more complicated than those in elemental metals, particularly the analysis of defects produced by ion irradiation is not straightforward.

The conventional theory of DXS uses analytical and numerical schemes to estimate the strain field around a defect and hence calculate the diffuse X-ray scattering [9,17]. While this approach has proven quite successful in many respects, it does have the drawback that each kind of defect has to be treated separately, and treating defects with a complicated structure and strain field is very difficult.

Another approach to obtaining the diffuse scattering is to do direct lattice sums, i.e. obtain the displacements of atoms around a defect and then obtain the scattering directly from the atom positions. Since the experimentally measurable

part of the scattering depends on the long-range strain field around a defect, this approach requires obtaining the displaced atom positions of at least a few hundred thousand atoms, and hence computer simulations. The approach of direct summation over lattice points was pioneered by Keating and Goland already around 1970 [18], but because of the limited computer capacity at the time the strain fields used were very simple. Two major developments since then make the lattice sum approach much more practical now. First, the dramatic increase in computer capacity makes it feasible to treat millions of atoms and their interactions at the same time. Second, many-body interatomic potentials which reproduce all first-order elastic constants to an accuracy of $\sim$10% now exist for most elemental crystals. Thus it is now possible to calculate a realistic strain field surrounding a defect by relaxing the atom positions of some 10^5 – 10^7 atoms around a defect. The relaxation is carried out by minimizing the potential energy of the system with respect to an interatomic potential describing the interactions between the atoms. This method has the major advantage that it can be applied in a straightforward way to defects in any material for which a good interatomic potential has been formulated. In the following section we will give a brief description of our method.

2.2. Atomistic analysis method

The X-ray intensity S close to a Bragg peak for a given scattering vector $\mathbf{K}$ for an arbitrary set of atom positions $\mathbf{R}_i$ in an infinite monatomic crystal can be written

$$S(\mathbf{K}) = \left| f_{\mathbf{K}} \sum_i \mathrm{e}^{\ \sigma^2 \mathbf{R}_i^2/2a^2} \mathrm{e}^{i\mathbf{K}\cdot\mathbf{R}_i} \right|^2, \qquad (1)$$

where σ corresponds to the resolution of the experiment and f_K is the atomic form factor [9,18,19]. The diffuse scattering from a defect is determined by the strain field around the defect, which enters the above expression as small displacements in the atom positions $\mathbf{R}_i$. In principle, if the atom positions of a defect and all surrounding atoms are known, the scattering can be calculated directly from this expression. The work of Keating [18] and our experience has shown that for values of σ corresponding to experimental resolutions the number of atoms needed to evaluate Eq. (1) typically is of the order of 10^6–10^8. This number, while large, is not necessarily prohibitive with modern computational capacity and linear algorithms.

The relaxation of atom positions is carried out by minimizing the total energy of a system of atoms with repect to the Stillinger–Weber interatomic potential [20]. Since this potential reproduces the elastic constants of silicon to an accuracy of 20% or better [21], and is also fit to far-from-equilibrium properties, it can be assumed to produce a realistic strain field both close and far from the defect. We emphasize that the potential does not necessarily give the correct structure for any given defect. However, it can still be used to obtain an understanding of how the DXS changes with increasing defect size – even though the potential may not give the right structure for, say, a tetrainterstitial, the calculation still gives an idea of how the scattering from a small interstitial cluster differs from that of an interstitial. This kind of accuracy is sufficient at the present, rather qualitative level of the analysis. It is possible, however, to combine atomic coordinates for the defect center obtained from realistic ab initio calculations with positions calculated using a classical potential outside the defect core.

We use two ways for obtaining the atom positions necessary for calculating the DXS. In the simpler one we place a defect in the center of a large sphere, relax all atoms in the sphere to their potential energy minimum, and then calculate the sum over atom positions which gives the diffuse scattering. While this scheme is straightforward, it has the limitation that one needs to have the positions of all atoms in the sphere in computer memory at the same time. Hence the amount of atoms which can be treated is limited by the available capacity. In practice, some 10 million atoms can be handled on a fast single-processor present-day computer with a few gigabytes of memory. The limit in the number of atoms limits how close to the Bragg peak the DXS distribution can be obtained.

To overcome this limit, we have developed an extrapolation scheme which allows obtaining the

diffuse scattering arbitrarily close to the Bragg peak. In this scheme, we obtain the shape of the strain field from a relaxation of a few hundred thousands of atoms, then use the shape of the strain field to obtain the displacement of a single atom far from the defect. In this way the positions of only a few hundred thousand atoms need to be stored in computer memory at the same time, and the extrapolation can be carried out arbitrarily far from the defect. This method also has the advantage that possible errors arising from atom relaxation at the surface of the sphere are subtracted out. The extrapolation method has been described in detail elsewhere [22].

The results of the two simulation methods are in excellent qualitative agreement. In some cases there are small quantitative differences in the results arising from numerical inaccuracies, but these are inconsequential at the present level of accuracy of the analysis.

2.3. Simulation results

We will present both the simulation and experimental results in plots of Sq^2 versus q, where S is the scattering intensity and q is the distance to the center of the Bragg peak in reciprocal space. For reasons which become apparent below we have found that this way of plotting the results makes it easy to make qualitative conclusions of the nature of defects directly from the scattering.

The results obtained from the simulations have, in all cases where a relevant comparison is possible, been in good agreement with the classical theory of DXS. For instance, the simulations are consistent with the prediction that the integrated diffuse scattering intensity of a defect is proportional to the square of the relaxation volume of the defect [8]. Also, the symmetric part of the scattering from a single interstitial or vacancy is proportional to $q^{\ 2}$ close to the Bragg peak, in agreement with the Huang prediction. The method also gives the correct shape of the scattering for the dumbbell interstitial in FCC metals [23]. For defect clusters, we do not observe parts with a well-defined $q^{\ 2}$ and $q^{\ 4}$ symmetric part of the scattering predicted by the Huang and Stokes–Wilson approximations [9]. Instead, the "exponent" of the q dependence varies smoothly with q. This is one reason why we prefer presenting the results in Sq^2 plots. The location of the maximum in these plots is straightforward to recognize and corresponds to the cluster size.

We have also used the simulations to test whether surface effects can affect the diffuse scattering significantly. The most important result is that surface effects in the diffuse scattering of in-plane peaks are negligible for defects deeper than 3 nm from the surface. Details of these calculations will be presented elsewhere.

In the present article, we will only present results of radial scans over a Bragg peak. While these results do not reveal the exact structure of a defect, they are highly useful in examining the cluster sizes and the separation between interstitials and vacancies in Frenkel pairs. Calculations of two-dimensional intensity distributions in reciprocal space can be useful in examining the exact structure of a single kind of defect, but are difficult to use for the complicated ion-irradiation induced damage dealt with now.

Fig. 1 shows results of DXS calculations for radial scans of vacancy clusters. The Bragg peak has been left out from the center since it is not relevant in the present context. The width of the

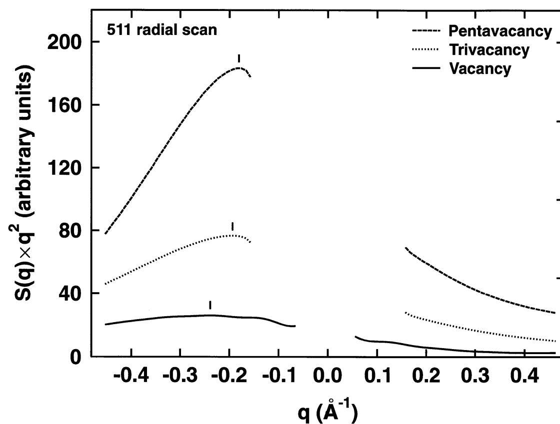

Fig. 1. Simulated diffuse scattering for three vacancy clusters. The Bragg peak has been left out of the figure. The locations of the maxima on the negative side are indicated by tiny vertical lines. The relaxation volumes of the mono-, tri- and pentavacancy used here are −1.5, −3.2 and −5.3 atomic volumes, respectively.

Bragg peak depends on the σ parameter, which was between 0.05 and 0.15 in these calculations. The intensity is plotted as Sq^2, where q is the distance to the Bragg peak in reciprocal space. We see that the scattering for all the vacancy clusters is stronger on the negative side of the Bragg peak, as expected from theory [9]. The locations of the maxima on the negative side in this Sq^2 plot are proportional to the defect size; the larger the defect relaxation volume, the closer the maximum is to the Bragg peak located at $q = 0$. Also, the decrease of the scattering beyond the maximum is more rapid for larger defects, corresponding to q exponents smaller than -2, as predicted by theory for defect clusters.

The scattering from interstitial clusters is illustrated in Fig. 2. The shape of the scattering is essentially a mirror image of that for vacancy clusters. The scattering is stronger on the positive side, and the maximum shifts towards the Bragg peak with increasing defect size.

The same behavior was seen for larger interstitial and vacancy clusters as well, up to clusters consisting of 64 defects (with relaxation volumes of roughly 50 atomic volumes). The integrated diffuse scattering was on average proportional to the square of the relaxation volume of the defect, as expected [9], but individual defects could deviate somewhat from this average trend.

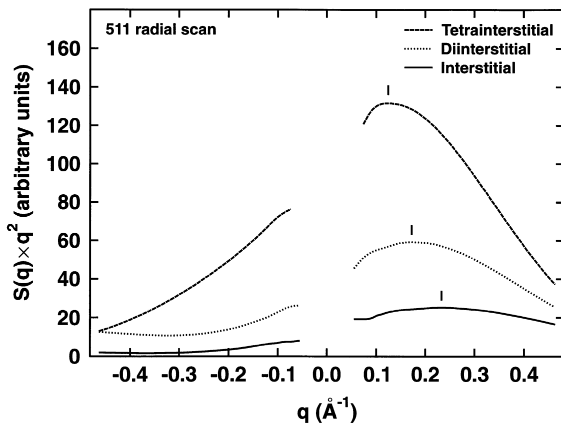

Fig. 2. Simulated diffuse scattering for three interstitial clusters. The Bragg peak has been left out of the figure. The locations of the maxima on the positive side are indicated by tiny vertical lines. The relaxation volumes of the mono-, di- and tetrainterstitial used here are +1.5, +2.6 and +4.3 atomic volumes, respectively.

Damage clusters of other kinds, like amorphous zones and damage produced by collision cascades, exhibited similar behavior. Damage with a positive relaxation volume had strong scattering on the positive side, damage with a negative relaxation volume strong scattering on the negative side. Large amorphous zones produced sharp and distinct peaks in the scattering close to the Bragg peak. This is illustrated in Fig. 3, where the scattering from a few amorphous zones are presented. The "4 keV Au" is the damage produced by a 4 keV Au recoil in Si, which contains about 900 atoms and has a relaxation volume of $-30\ \Omega$, where Ω is the atomic volume (the negative sign of the relaxation volume is due to inadequacies in the Stillinger–Weber potential description of a-Si). The 250-atom a-Si cluster has a relaxation volume of $+5.1\ \Omega$ and the 500-atom cluster one of $+10.7\ \Omega$, about corresponding to the experimental density of a-Si [24].

The common factor for the scattering from all amorphous clusters is that they exhibit strong scattering close to the Bragg peak. Note that the scattering for even the 250-atom zone is roughly a factor of 20 stronger than that of the single interstitial or vacancy (the intensity scales of the different simulation figures are comparable). The strength of the scattering is due to their large relaxation volumes, and the irregular shape of the

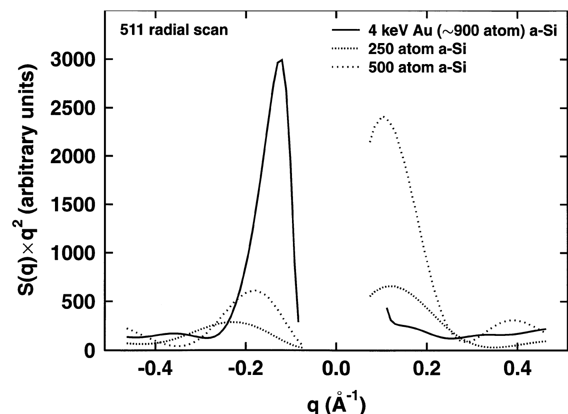

Fig. 3. Simulated diffuse scattering for a few amorphous clusters. The nature of the clusters is described in the text.

scattering due to the complex character of the amorphous–crystalline interface, which leads to an unsymmetric strain field.

The damage from Frenkel pairs has, not surprisingly, peaks on both sides of the Bragg peak. The calculated scattering from a few Frenkel pairs is illustrated in Fig. 4. The pairs are listed as a function of the separation between the interstitial and vacancy forming the pair. The scattering goes down close to the Bragg peak due to the cancellation of relaxation volumes and correlation effects between the interstitial and vacancy [8].

Analysis of the data shows that the separation between the peaks on the negative and positive side is inversely proportional to the distance between the vacancy and interstitial – the defect with a separation of 19 Å has two peaks close to the Bragg peak, whereas one of the peaks of the 5 Å pair extends outside the figure. Furthermore, comparison of the scattering calculated for different Bragg peaks showed that the separation between the peaks is about the same in units of q. This enables a rough determination of the average separation between the vacancy and interstitial that form the pair, in a similar manner as done by Ehrhart using classical methods [8].

Thus we conclude that the results of our simulations are well in line with what is expected from classical theory, but the ease at which the method can be used for new kinds of defects can make it highly useful for complex defects.

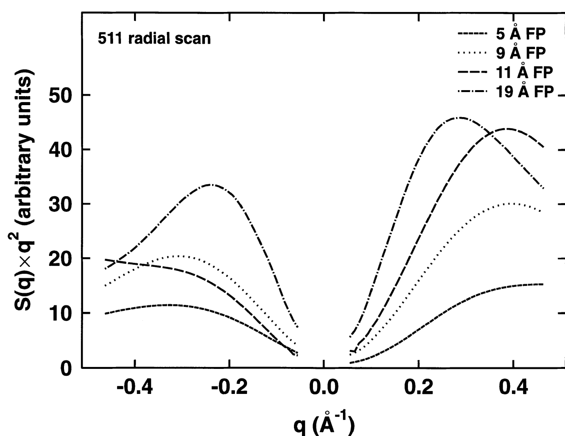

Fig. 4. Simulated diffuse scattering for four Frenkel pairs. The Frenkel pairs are labeled with the separation between the interstitial and vacancy that form the pair. The relaxation volumes of all pairs are close to zero.

3. Experimental results

As an example of how the information of simulations can be applied to analyze experimental DXS lineshapes, we summarize the experimental work of Partyka et al. [10,11] and compare the simulations to these results. A more comprehensive analysis will be presented elsewhere [11].

We have examined damage produced by 4.5 keV He and 20 keV Ga in silicon using DXS. Details of the experimental procedure are found elsewhere [10], but we present the most significant parts here. The silicon samples were phosphorus doped, Czochralski grown Si (1 1 1) wafers with miscut angles less than 0.1°, with resistivities of about 50 Ω cm. The two ions were chosen to provide a contrast between light ions presumably producing mostly Frenkel-pair-like damage, and a moderately heavy ion which is expected to produce amorphous zones [25,26]. The samples were implanted in situ with an ion gun in the X-ray scattering measurement chamber at the synchrotron at Brookhaven National Laboratory. The X-ray measurements were carried out at glancing angles to obtain sensitivity to close-to-surface defects. The sample could be cooled down to 100 K and measured in situ in the chamber between cooling and heating steps.

The DXS results of He implantation at 100 K as a function of dose is presented in Fig. 5. The background measured for the same sample before implantation has been subtracted from the data. The dose is given in units of displacements per atom (dpa), which is an estimate of the number of atomic displacements produced during the irradiation per lattice atom. The exact conversion factor between the real dose and dpa depended on the X-ray penetration depth, but rough values for the correspondence are dose $= 10^{16} \times$dpa for He and dose $= 2\times 10^{14} \times$dpa for Ga, where the dose is given in units of ions/cm^2 . The estimate was made using the TRIM92 computer code [27,28], and is thus based on a binary collision cascade

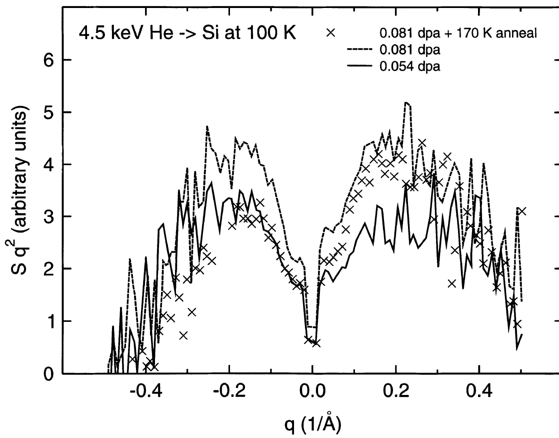

Fig. 5. Radial scan of diffuse scattering from He-implanted Si at 100 K for two different low doses, plotted in units of Sq^2 where S is the background subtracted scattering intensity. As expected, the intensity increases with the dose. Also shown is the signal for the dose of 0.081 dpa after an anneal at 170 K. The data are from Refs. [10,11].

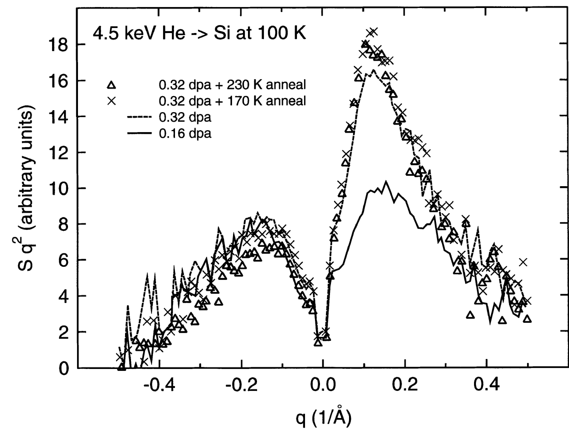

Fig. 6. Radial scan of diffuse scattering from He-implanted Si at 100 K for two different high doses. Also shown is the signal for the higher dose of 0.32 dpa after anneals at 170 and 230 K. The data are from Refs. [10,11].

approximation. Even though this description of course does not account for all important aspects of cascade development in Si [29,30], it does make different doses for Ga and He roughly comparable.

Comparison with Figs. 1–4 shows that the damage signal clearly resembles a Frenkel pair signal, with a separation of 1–2 nm between the interstitial and vacancy (as noted above, the q dependence of the scattering from different peaks is comparable when plotted in units of 1/ Å). From the present data we cannot exclude the possibility that small defect clusters are present, but comparison with Figs. 1 and 2 clearly shows that larger clusters (with more than ~4 defects) cannot be present in significant concentrations. We note that although it is not done here, it is possible to derive the defect concentrations from absolute values of the measurements.

Fig. 6 shows data for He implantations at higher doses. The maximum on the positive side has now clearly shifted inwards, and the signal on the positive side is clearly much stronger than that at the negative side at the highest dose of 0.32 dpa. The signal on the positive side clearly resembles that expected for interstitial clusters (cf. Fig. 2), and must be a result of cascade overlap at these high doses.

Fig. 7 illustrates the dose dependence for Ga implantations. As for the He implantations, the lowest-dose signal resembles that expected for Frenkel pairs or small defect clusters. For He this was expected, but for Ga one would expect to see a signal from amorphous clusters close to the Bragg peak [25]. Using molecular dynamics (MD) simulations of 20 keV Ga implantation and our DXS simulations we estimate that this signal

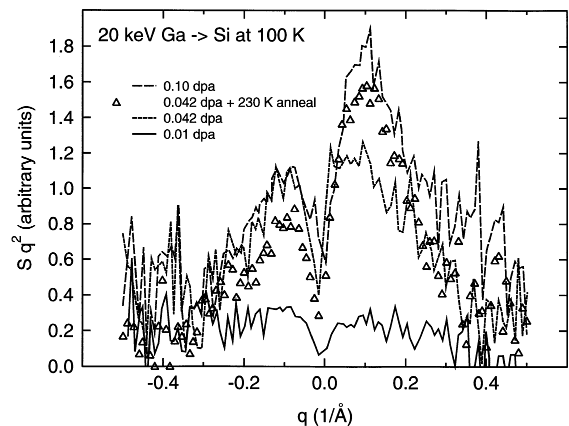

Fig. 7. Radial scan of diffuse scattering from Ga-implanted Si at 100 K. Also shown is the signal for the higher dose of 0.042 dpa after annealing at 230 K. The data are from Refs. [10,11].

should be roughly a factor of 2 stronger than the Frenkel pair signal. We did not observe such a signal in any of our experiments, however. There are at least three possible explanations to this. One is that the density of the amorphous pockets produced during irradiation is very close to zero, i.e. not the same as the experimental density of macroscopic a-Si which we used in our simulations [24]. The second is that the classical MD models overestimate the size of the amorphous clusters. We cannot rule this possibility out, but our recent comparison of different potentials indicates that this is unlikely [30]. The third is that the amorphous clusters do form, but anneal out in part or completely. Recent MD simulations indicate that amorphous clusters formed by heavy ions recrystallize at least in part even at moderate temperatures like 300 K [26], which could be enough to reduce the size of amorphous zones so that their DXS lineshape resembles small clusters. Although the present data is not conclusive regarding this question, we believe partial recrystallization of amorphous zones is the most likely explanation for the lack of an amorphous-zone signal.

As for He, the high-dose data for the Ga implantation has a strong signal on the positive side, indicative of interstitial clustering. Although the strong signal on the positive side could also derive from amorphous clusters, the observation of an increase in cluster size during annealing (see below) makes this explanation unlikely. Fig. 8 shows DXS measurements of Ga implantation at 150 K to even higher doses. Here the very highest dose (0.12 dpa) is actually weaker than that of the previous dose of 0.04 dpa. This is an indication of amorphization of the implanted regions (an amorphous sample produces no distinct DXS signal close to the Bragg peak). The dose at which this occurs ($\sim 2\times 10^{13}$ ions/cm^2) is consistent with amorphization doses obtained by other methods [31], and the occurrence of amorphization was verified using RBS-channeling measurements. Hence the data indicates that the amorphization of silicon during ion irradiation proceeds homogeneously through the buildup of interstitial clusters and a subsequent collapse to an amorphous state.

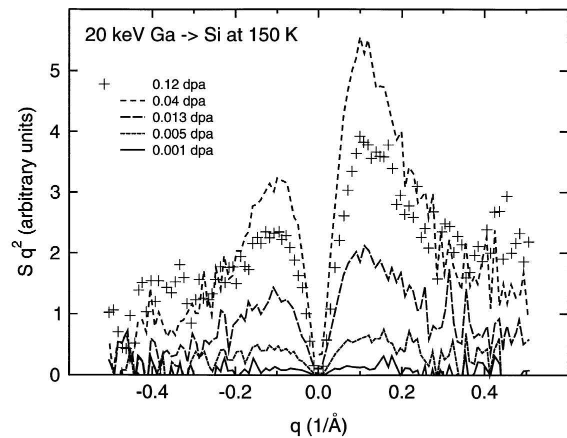

Fig. 8. Radial scan of diffuse scattering from Ga-implanted Si at 150 K. Note that the highest-dose distribution of 0.12 dpa (plotted with "+" signs) is weaker than the 0.04 dpa one, indicating amorphization of the film. The data are from Refs. [10,11].

Figs. 5–7 also show data of annealing steps from 100 to 170 and 230 K. For both He and Ga, the annealed curves are as strong or stronger on the positive side, and weaker on the negative than the unannealed data. This growth of interstitial cluster indicates that the silicon interstitial becomes mobile between 100 and 170 K. Some of the mobile interstitials annihilate with vacancies or vacancy clusters, and some become part of interstitial clusters. The former effect decreases the vacancy cluster signal. Since the strength of the DXS signal is proportional to the square of the relaxation volume, the later effect can increase the interstitial cluster signal even though the total number of defects decreases due to the mobility. These effects are not very pronounced, though, likely because many of the interstitials are already trapped in immobile defect clusters.

We also examined the damage introduction efficiency as a function of dose and temperature. The introduction efficiency for He implants goes down dramatically between 100 and 210 K. The most likely explanation is the recombination of close Frenkel pairs during the higher-temperature irradiation, although interstitial mobility also may play a role. A similar, albeit not as dramatic,

difference in damage introduction rate was observed for Ga irradiations as well. Since Ga irradiation is expected to produce more clusters than He, the smaller difference between 100 and 210 K is expected. These results, moreover, indicate that at least the 100 K data is not dependent on reactions between self-defects and impurities in the Si.

4. Discussion

The experimental results described above can be summarized in terms of four quantities: interstitial mobility, vacancy mobility, Frenkel pair recombination and amorphization mechanism. In the following we discuss how our results relate to results by others in the literature. Since most experimental methods depend on the electrical structure of defects, whereas ours does not, the comparison is not necessarily direct. The DXS method should see all defects present in the lattice regardless of their charge state or levels in the gap, whence it can provide a test on whether previous measurements have observed all defects. Indeed, the DXS measurement of Ehrhart indicate that electron irradiation can cause a large number of close Frenkel pairs not visible by other methods [8].

Our observation of an increase in interstitial cluster size between 100 and 170 K provides evidence that the silicon self-interstitial becomes mobile in this temperature range (at least for the kind of highly ohmic silicon resulting from ion irradiation). Since interstitials are hard to detect by the most common methods used to study silicon defects (EPR, DLTS and positron measurements), most previous deductions on their mobility at low temperatures are indirect. In a recent review on EPR and DLTS results, Watkins states that the interstitial is mobile below 4 K in p-type Si during electron irradiation, and at about 140 K in n-type Si [6]. It is not clear whether these experiments are comparable to the highly ohmic Si produced during ion irradiation, but the EPR result in n-type silicon is very close to our result.

Vacancies are generally believed to be mobile below room temperature, and numerous studies have observed divacancies in the temperature range 100–300 K [7,32–35]. EPR results indicate that vacancies become mobile around 70 K at room temperature in n-type Si [6]. Our results are not conclusive on this point. We do not see vacancy mobility in this temperature range, but cannot presently deduce whether the Frenkel-pair-like signal derives from simple Frenkel pairs or divacancy-interstitial complexes formed by vacancies mobile at 100 K.

We observed a very strong decrease in the damage formation efficiency between 100 and 210 K both for He and Ga irradiations. This indicates that most of the close pairs anneal out at the higher temperatures, and agrees with the thermally activated annealing of Frenkel pairs observed recently by Ehrhart during electron irradiation [8]. Our effect is much stronger, though, roughly two orders of magnitude for He and one order of magnitude in Ga [10]. This is probably a consequence of the much higher damage level during our ion irradiations than in low-dose electron-irradiations where much of the damage is trapped at impurities. The observation of a large number of close (possibly electrically inactive) Frenkel pairs annealing below room temperature is a likely explanation to DLTS measurements at room temperature seeing much less damage than predicted by ballistic models [35].

Our observation that the amorphization of silicon proceeds through the buildup of interstitial clusters provides one of the first direct experimental indications of a homogeneous amorphization mechanism in silicon. It also agrees well with several previous experiments and simulations suggesting this mechanism. The MD cascade simulations by Caturla and Diaz de la Rubia indicate that heterogeneous amorphization is not possible above 600 K [26]. Lewis and Nieminen conclude from MD simulations that amorphization can be induced by point defects *provided* they form clusters. Although amorphous clusters in silicon have been seen directly by electron microscopy and found to be stable at room temperature by Ruault et al., one of the papers presenting this result concludes that the amorphous zones observed are not sufficiently large to explain the amorphization [36].

5. Conclusions

In the present work we have shown that atomistic analysis of glancing incidence diffuse X-ray scattering data is a viable method for directly observing many kinds of defect structures in silicon.

Our results on He and Ga irradiation of Si provide evidence that the self-interstitial becomes mobile around 150 K in ion-irradiated silicon. It also indicates that much of the damage produced during irradiation is in the form of close Frenkel pairs (or close divacancy-interstitial complexes), most of which recombine above 100 K. Finally, the results indicate that the amorphization of silicon proceeds through the homogeneous buildup of interstitial clusters and a subsequent "collapse" to the amorphous state.

Acknowledgements

The research was supported by the US Department of Energy, Basic Energy Sciences under grant DEFG02-91ER45439, and the Academy of Finland. Ggrants of computer time from the National Energy Research Computer Center at Livermore, California, the NCSA at Urbana-Champaign, Illinois, and the Center for Scientific Computing in Espoo, Finland, are gratefully acknowledged.

References

[1] D.J. Eaglesham, P.A. Stolk, H.-J. Gossmann, T.E. Haynes, J.M. Poate, Nucl. Instr. and Meth. B 106 (1995) 191.
[2] R. Car, P. Blochl, E. Samrgiassi, Mater. Sci. Forum 83–87 (1992) 433.
[3] M.J. Puska, S. Pöykkö, M. Pesola, R.M. Nieminen, Phys. Rev. B 58 (1998) 1318.
[4] W. Taylor, B.P.R. Marioton, T.Y. Tan, U. Gösele, Radiat. Effect. Def. Solid. 111/112 (1989) 131.
[5] M. Tang, L. Colombo, J. Zhu, T. Diaz de la Rubia, Phys. Rev. B 55 (1997) 14279 and references therein.
[6] G.D. Watkins, in: T. Diaz de la Rubia, S. Coffa (Eds.), Defects and Diffusion in Silicon Processing, vol. 469, MRS Symposium Proceedings, Materials Research Society, Pittsburgh, PA, 1997, p. 139.
[7] H. Kauppinen, C. Corbel, K. Skog, K. Saarinen, T. Laine, P. Hautojärvi, P. Desgardin, E. Ntsoenzok, Phys. Rev. B 55 (1997) 9598.
[8] P. Ehrhart, H. Zillgen, in: T. Diaz de la Rubia, S. Coffa (Eds.), Defects and Diffusion in Silicon Processing, vol. 469, MRS Symposium Proceedings, Materials Research Society, Pittsburgh, PA, 1997, p. 175.
[9] P.H. Dederichs, J. Phys. F: Metal Phys. 3 (1973) 471.
[10] P. Partyka, Ph.D. Thesis, University of Illinois at Urbana-Champaign, Urbana, IL, 1997.
[11] P.J. Partyka, K. Nordlund, Y. Zhong, I.K. Robinson, R.S. Averback, P. Ehrhart, to be published.
[12] P. Ehrhart, K.H. Robrock, H.R. Shober, in: R.A. Johnson, A.N. Orlov (Eds.), Physics of Radiation Effects in Crystals, Elsevier, Amsterdam, 1986, p. 3.
[13] H. Zillgen, P. Ehrhart, Nucl. Instr. and Meth. B 127/128, (1996) 27.
[14] K. Karsten, P. Ehrhart, Phys. Rev. B 51 (1995) 10508.
[15] W. Mayer, H. Peisl, J. Nucl. Mater. 108/109 (1982) 627.
[16] S. Grotehans, G. Wallner, E. Burkel, H. Metzger, J. Peisl, H. Wagner, Phys. Rev. B 39 (1989) 8450.
[17] P. Ehrhart, H. Trinkaus, B.C. Larson, Phys. Rev. B 25 (1982) 834.
[18] D.T. Keating, A.N. Goland, Acta Cryst. A 27 (1971) 134.
[19] In the present description of the analysis method we neglect the atomic form factor for simplicity.
[20] F.H. Stillinger, T.A. Weber, Phys. Rev. B 31 (1985) 5262.
[21] H. Balamane, T. Halicioglu, W.A. Tiller, Phys. Rev. B 46 (1992) 2250.
[22] K. Nordlund, P. Partyka, R.S. Averback, in: T. Diaz de la Rubia, S. Coffa (Eds.), Defects and Diffusion in Silicon Processing, vol. 469, MRS Symposium Proceedings, Materials Research Society, Pittsburgh, PA, 1997, p. 199.
[23] P.J. Partyka, R.S. Averback, K. Nordlund, I.K. Robinson, D. Walko, P. Ehrhart, T. Diaz de la Rubia, M. Tang, in: I.M. Robertson, G.S. Was, L.W. Hobbs, T. Diaz de la Rubia, Microstructure Evolution During Irradiation, vol. 439, MRS Symposium Proceedings, Materials Research Society, Pittsburgh, PA, 1997, p. 89; the same paper is also published in MRS Symp. Proc., vol. 438, p. 77.
[24] J.S. Custer, M.O. Thompson, D.C. Jacobson, J.M. Poate, S. Roorda, W.C. Sinke, F. Spaepen, Appl. Phys. Lett. 64 (1994) 436.
[25] T. Diaz de la Rubia, G.H. Gilmer, Phys. Rev. Lett. 74 (1995) 2507.
[26] M.J. Caturla,, L.A.M.T. Diaz de la Rubia, G.H. Gilmer, Phys. Rev. B 54 (1996) 16683.
[27] J.F. Ziegler, TRIM-92 computer code, private communication, 1992.
[28] J.P. Biersack, L.G. Haggmark, Nucl. Instr. and Meth. 174 (1980) 257.
[29] M.J. Caturla, V. Konoplev, I. Abril, A. Gras-Marti, Nucl. Instr. and Meth. B 102 (1995) 19.
[30] K. Nordlund, M. Ghaly, R.S. Averback, M. Caturla, T. Diaz de la Rubia, J. Tarus, Phys. Rev. B 57 (1998) 7556.

[31] J.R. Dennis, E.B. Hale, J. Appl. Phys. 49 (1978) 1119.
[32] B.G. Svensson, C. Jagadish, J.S. Williams, Phys. Rev. Lett. 71 (1993) 1860.
[33] O.W. Holland, M.K. El-Ghor, C.W. White, Appl. Phys. Lett. 53 (1988) 1282.
[34] J.L. Benton, S. Libertino, P. Kringhøj, D.J. Eaglesham, J.M. Poate, J. Appl. Phys. 82 (1997) 120.
[35] S. Libertino, J.L. Benton, S. Coffa, D.C. Jacobsen, D.J. Eaglesham, J.M. Poate, M. Lavalle, P.G. Fuochi, in: T. Diaz de la Rubia, S. Coffa (Eds.), Defects and Diffusion in Silicon Processing, vol. 469, MRS Symposium Proceedings, Materials Research Society, Pittsburgh, PA, 1997, p. 139.
[36] M.O. Ruault, J. Chaumont, J.M. Penisson, A. Bourret, Phil. Mag. A 50 (1984) 667.